# Face stability of slurry shield-driven tunnel in an aquifer

W. H. Zhou, T. Xu
*Department of Civil and Environmental Engineering, University of Macau, Macao, China*

A. Bezuijen
*Department of Civil Engineering, Ghent University, Ghent, Belgium & Deltares, Delft, The Netherlands*

ABSTRACT: In this article the face stability of slurry shield-driven tunnel in an aquifer is investigated. The influences of slurry infiltration at the face and soil layering are taken into account. The results show that due to the infiltration an additional margin for the support pressure is required. At larger slurry infiltration distance or larger cover depth to tunnel diameter ratio (*C*/*D*), a higher margin is required. It also appears that soil layering affects the hydraulic gradient that stabilise the face of cohesionless soil. TBM excavation in a semi-confined aquifer (compared to an unconfined aquifer) leads to higher excess pore water pressures in the soil around the TBM and a reduced infiltration of slurry into the soil in front of the TBM. The excess pore water pressures in a semi-confined aquifer are present over a larger area than in an unconfined aquifer, increasing the risk of a blow-out during excavation.

## 1 INTRODUCTION

The tunnel-boring machine (TBM) tunnelling technique has been developed to construct tunnels that require strict settlement control, e.g. in urban areas with a large amount of buildings, historic areas etc., or where the soil is very soft (e.g. when crossing a river or estuary). When TBM tunnelling is performed below the water table, especially in cohesionless soil with high water pressure, effective support at the face plays a key role in the face stability. Practice proved that, in such a condition, support suspension without additive(s) is insufficient to stabilise the face (Bezuijen, 1996; Hölscher, 2008), and may lead face collapse. If the face pressure is higher than the pore pressure in the soil, there will be no flow into the excavation chamber. However, the face will not be stable, because the hydraulic gradient is too low (Van Rhee & Bezuijen, 1992). The face stability and limitation of the groundwater flow have to be achieved by pressurising the bentonite slurry for slurry TBM or foam for earth-pressure-balance shield (EPB shield) at the face. It should also be noted that too large slurry or foam pressure may lead to face blow-out. Therefore, carefully determining the support pressure is important. Various methods in analysing face stability and determining the minimal and maximum support pressures can be found in literature, such as limit equilibrium analysis (Horn, 1961; Jancsecz & Steiner, 1994; Qarmout et al. 2019), numerical modelling (Zhang et al. 2015; Liu et al. 2019), physical modeling (Chambon et al. 1991; Ahmed & Iskander, 2012; Chen et al. 2013). Just little attention was given to the infiltration of support suspension in existing literature (e.g. Bezuijen et al. 2001; Broere, 2001; Broere & van Tol, 2001; Broere, 2015).

Due to the pressure difference between the excavation chamber of the TBM and the ground, support suspension will infiltrate into the soil and thus there will be a flow in front of the face. In such a situation, part of support pressure applied through the support suspension at the tunnel face will transfer into excess pore water pressure in the soil. The induced lowering of effective support pressure should be avoided (Broere, 2015). However, this is hard to be achieved.

This study therefore aims to investigate the effectiveness of the support, global stability of the face under infiltration of slurry into the soil ahead of the tunnel face and soil layering and seepage and their influences on the macro- and micro-stability of the face. The study focuses on slurry shields, but the findings are also valid for earth-pressure-balance shields (EPB shields).

## 2 MACRO-STABILITY OF THE FACE

### 2.1 *Basic framework*

The basic framework for analysing the face stability considering the effect of infiltration is based on the

wedge model that first proposed by Horn (1961), and then followed by many others (e.g. Anagnostou & Kovari; 1994; Jancsecz & Steiner, 1994; Broere, 2001; Broere & van Tol, 2001; Perazzelli et al. 2014; Broere, 2015). Figure 1 shows a sketch of the basic framework of the model of face stability. The support pressure $E(\vartheta)$ is derived from the equilibrium of forces that act at the wedge as shown in Figure 2 (Broere, 2015):

$$E(\vartheta)=\frac{(G+P_v)(\sin\vartheta-\cos\vartheta\cdot\tan\phi_2')-2T-c_2\dfrac{D^2}{\sin\vartheta}}{\sin\vartheta\cdot\tan\phi_2'+\cos\vartheta} \quad (1)$$

where $G$ is the weight of the soil wedge (kN), $P_v$ is the vertical load from the soil prism (kN), $\vartheta$ is the sliding angle between the wedge and the horizontal plane (°), $\phi$ is the friction angle (°), $c_2$ is the cohesion (kPa) of soil in the tunnel face area, $T$ is the shear resistance force on the vertical triangular plane of the wedge (kN), and $D$ is the tunnel diameter (m).

The maximum support pressure can be determined by derivation of $E(\vartheta)$ to $\vartheta$:

$$\frac{\mathrm{d}\,E(\vartheta_{cr})}{\mathrm{d}\,\vartheta_{cr}}=0 \quad (2)$$

where $\vartheta_{cr}$ is the critical sliding angle (°).

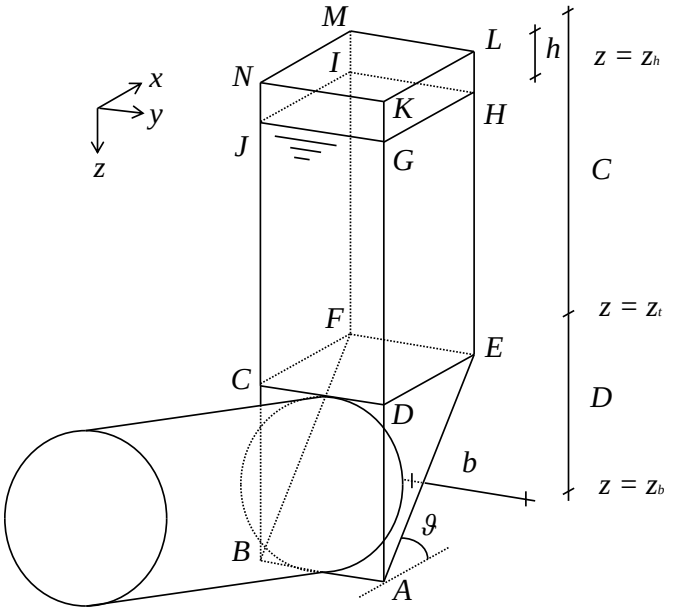


Figure 1. Wedge stability model (Broere, 2015)

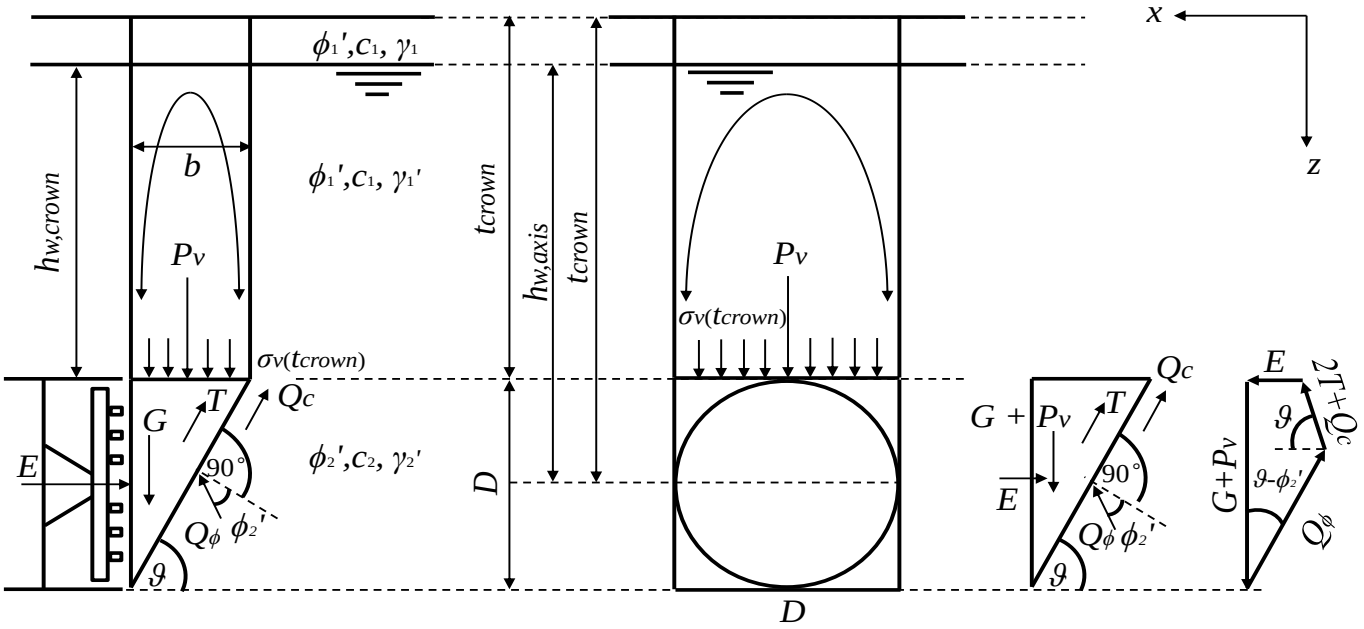


Figure 2. Equilibrium of forces that act at the wedge (modified after Zizka & Thewes, 2016).

The forces acting on the wedge can be obtained as follows:

Weight of the wedge:

$$G=\frac{1}{2}\frac{D^3}{\tan\vartheta_{cr}}\gamma_{2,av} \quad (3)$$

with $\gamma_{2,av}$ being the average unit weight of the soil in the tunnel face area (kN/m$^3$).

Vertical load from the soil prism:

$$P_v=\sigma_{v,crown}\frac{D^2}{\tan\vartheta_{cr}} \quad (4)$$

with $\sigma_{v,\,crown}$ the total vertical stress in tunnel crown (kPa).

$$\sigma_v(z)=\gamma_{1,av}\cdot z\ ,\ t_{crown}\ \leqslant\ 2D \quad (5a)$$

with $\gamma_{1,av}$ the average unit weight of the soil in the tunnel crown (kN/m$^3$).

$$\sigma_v = \frac{\frac{A}{U}\gamma_{1,av} - c}{K_1 \tan\varphi_1'}\left(1 - e^{-\frac{U}{A}K_1 \cdot z \cdot \tan\varphi_1'}\right) + \sigma_s e^{-\frac{U}{A}K_1 \cdot z \cdot \tan\varphi_1'}, \; t_{crown} > 2D \quad (5b)$$

where $A$ is the cross-sectional area of the silo ($m^2$); $U$ the circumference length of the silo (m); $K_1$ the coefficient of the lateral earth pressure in the area of the soil prism (-).

Resistance force on the vertical triangular plane of the wedge is:

$$T = T_R + T_c = \frac{c_2 \cdot D^2}{2 \cdot \tan\theta_{cr}} + \tan\varphi_2' K_2 \left(\frac{D^2 \cdot \sigma_v(t)}{2\tan\theta_{cr}} + \frac{D^3 \cdot \gamma_2}{6\tan\theta_{cr}}\right) \quad (6)$$

with $K_2 = \frac{K_0 + K_a}{2} = \frac{\tan\left(45^\circ - \varphi'/2\right)^2 + 1 - \sin\varphi_2'}{2}$, $K_0$ is the coefficient of lateral earth pressure at rest (-) and $K_a$ is the coefficient of Rankin's active earth pressure (-).

## 2.2 *Effective support ratio*

As pointed by Bezuijen et al. (2016) and Xu & Bezuijen (2019), during excavating, the advancement rate of TBM partially determines the face stability. There is a critical velocity that the advancement rate is equal to the infiltration velocity. If the advance rate is slower than the infiltration velocity, the assumption that a filter cake is formed during drilling is valid. If the advancement rate of the TBM is higher than the infiltration velocity, the cutting wheel of the TBM will cut off the all the slurry infiltrated soil and some non-infiltrated soil and carry it into the excavation chamber. In both situations, soil-slurry-mixture rather than 'clean slurry' will be present in the gap between the face and the excavation chamber. Hence, depending on the density of the slurry, there will be either no filter cake or a little filter cake formation at the face but a continuous infiltration (Xu & Bezuijen, 2019). For low infiltration rates the pressure in the soil close to the TBM is equal to face pressures. For higher infiltration rates there is still excess pore water pressure in the soil, but it is now determined by the TBM:

$$\phi = \frac{2n \cdot v_p}{D} \quad (7)$$

with $n$ the porosity of the soil (-); $v_p$ the pore fluid velocity (m/s) and $D$ the tunnel diameter (m).

As a result, part of support pressure will be transferred into excess pore water pressure (Bezuijen et al. 2001; Broere, 2001; Xu & Bezuijen, 2018). The net force acts at the face to support the wedge therefore is less, see Figure 3. Bezuijen et al. (2001) argued that the support is less effective in the situation with excess pore water pressure. The excess pore pressure will also create a vertical gradient over the block CDEFKLMN (see Figure 3) resulting in a reduction of the force from this block on the triangle. COB (2000) and Broere (2001) showed a significant increase in the minimum allowable tunnel face pressure to achieve a stable front, for the cases of the Second Heinenoord Tunnel and Botlet Rail Tunnel.

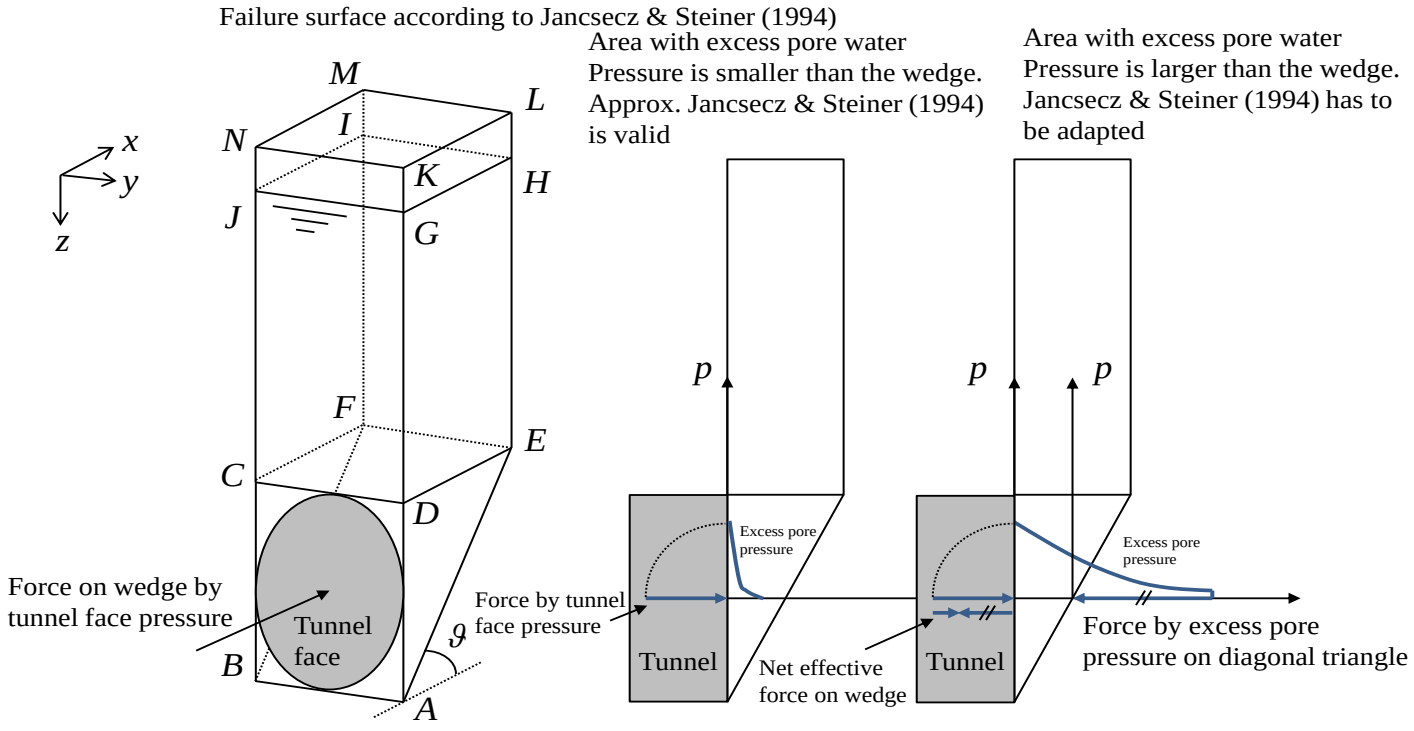


Figure 3. Pressure distribution over infiltration zone and excess pore water pressure (modified after Bezuijen, 2001)

Zizka & Thewes (2016) proposed a concept for the global stability of the wedge, namely the factor ($F$) defined as a ratio of area of the infiltrated zone and the wedge:

$$F = \frac{S_w}{S_e} = 1 - \frac{e_{\max,\text{invert}} \cdot h}{\left(e_{\max,\text{crwon}} + e_{\max,\text{invert}}\right) \cdot D} \tag{8}$$

where $S_e$, $S_w$ are the area of infiltrated zone within the wedge and the area of the total infiltrated zone ($m^2$); $e_{\max,\text{crown}}$, $e_{\max,\text{invert}}$, the maximum infiltration distance in crown and invert (m). The maximum infiltration distance ($e_{\max}$) during mud spurt can be determined by the infiltration tests (Xu & Bezuijen, 2019a).

Here, a more general expression is given. As shown in Figure 4, the two lines, the inclined sliding line (L1) and the front infiltration line (L2) are:

$$\text{L1: } y = \frac{D}{e_{\max,\text{invert}} - e_{\max,\text{crown}}}\left(e_{\max,\text{crown}} - x\right) \tag{9a}$$

$$\text{L2: } y = \left(\tan\vartheta\right)x - D \tag{9b}$$

The joint point of L1 and L2 is ($x_0$, $y_0$):

$$x_0 = \frac{\alpha e_{\max,\text{invert}}}{\tan\vartheta + \alpha} \tag{10a}$$

$$y_0 = \alpha\left(e_{\max,\text{crown}} - \frac{\alpha e_{\max,\text{invert}}}{\tan\vartheta + \alpha}\right) \text{ or } y_0 = \tan\vartheta\left(\frac{\alpha e_{\max,\text{invert}}}{\tan\vartheta + \alpha}\right) - D \tag{10a}$$

with $\alpha = \dfrac{D}{e_{\max,\text{invert}} - e_{\max,\text{crown}}}$.

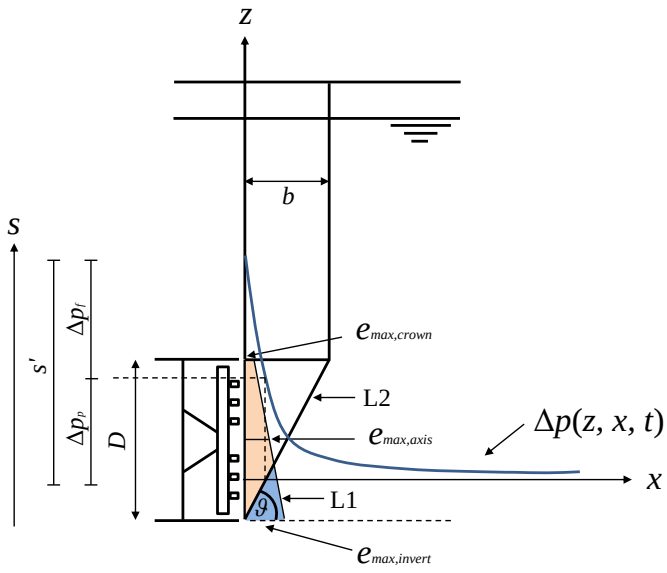


Figure 4. Influence of infiltrated zone in the global stability

As the pressure is linear along the depth, we have:

$$\frac{e_{\max,\text{crown}}}{e_{\max,\text{invert}}} = \frac{\Delta p}{\Delta p + \gamma_w \cdot D} \tag{11}$$

The areas that infiltrated zone within the wedge ($S_w$) and the total infiltrated zone ($S_e$) are:

$$S_e = \frac{1}{2}\left(e_{\max,\text{invert}} + e_{\max,\text{crown}}\right) \cdot D \tag{12}$$

$$S_w = S_e - \frac{1}{2} e_{\max,\text{invert}}\left(D - |y_0|\right), \; e_{\max,\text{crown}} < D\cot\vartheta \tag{13a}$$

$$S_w = \frac{1}{2} D^2 \cot\vartheta, \; e_{\max,\text{crown}} \geqslant D\cot\vartheta \tag{13b}$$

## 2.3 *Case study*

To investigate the effects of the infiltration distance, soil strength, tunnel diameter and cover depth on the effective support ratio, a case study of a tunnel bored in a homogeneous soil is presented: tunnel diameter $D$ = 10 m, cover depth $C$ = 20 m, slurry pressure $\Delta p$ = 50 kPa, water table depth $h$ = 3 m, effective specific weight $\gamma'$ = 11 kN/$m^3$, dry specific weight $\gamma_d$ = 17 kN/$m^3$, saturated specific weight $\gamma_s$ = 21 kN/$m^3$, cohesion $c$ = 0 kPa, friction angle $\phi$ = 36°. Equations (8) to (13b) based on Figure 4 are used to calculate the effective support ratios. This is valid during standstill, but not during drilling.

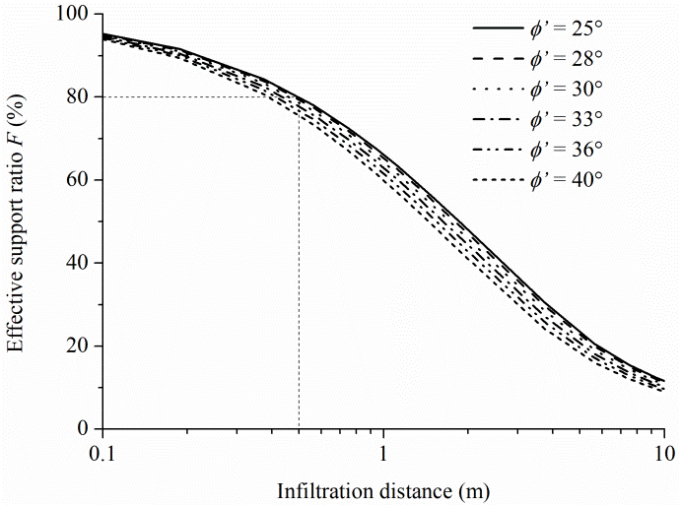


Figure 5. Effective support ratio with infiltration distance for various friction angles

Figure 5 shows that infiltration distance has significant influence in the effective support that acts at the tunnel face. For small infiltration distances only (< 0.5 m), the effective support ratio is high (> 80 %). For large infiltration distance (> 6.0 m), the effective support ratio (< 20%) can be neglected. The results were based on the low viscosity of support suspension. Support suspension of higher viscosity can lead to a shorter infiltration distance and hence a higher effective support ratio. Also for a low soil permeability the effective support ratio is limited, but now because of excess pore water pressure. Furthermore, the internal friction angle of the soil in

front of the face has limited influence in the effective support ratio because the induced change in sliding angle caused by is small, see Figure 6.

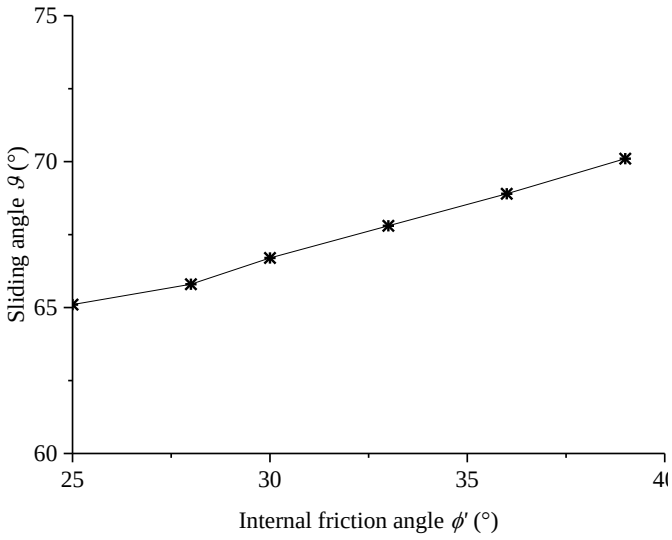


Figure 6. Sliding angle against internal friction angle of the soil in front of the tunnel face

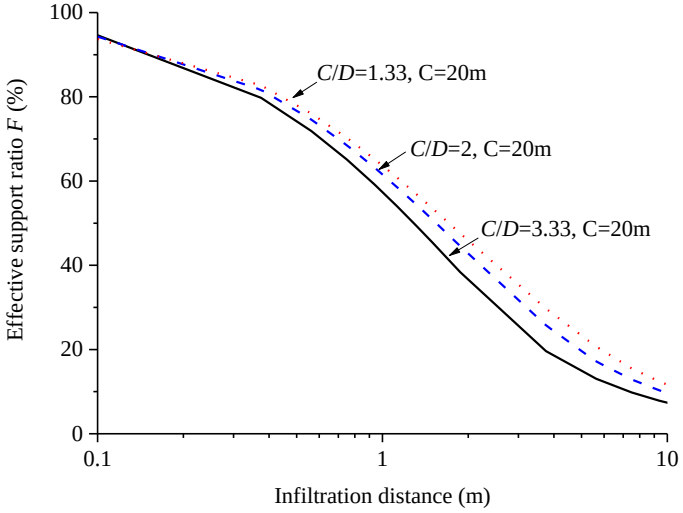


Figure 7. Effective support ratio with infiltration distance for various *C*/*D* with the constant *C* – coarse sand

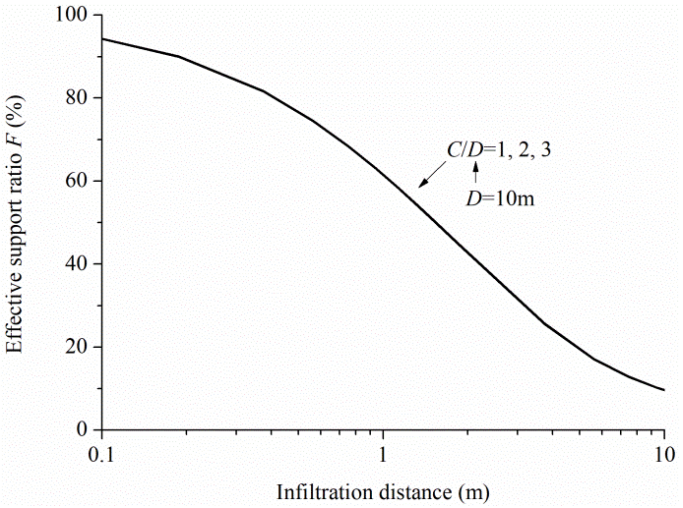


Figure 8. Effective support ratio with infiltration distance for various *C*/*D* with the constant *D*

Cover depth and tunnel diameter may influence the required support pressure too. For coarse sands shown in Figure 7, a larger value of *C*/*D* results in smaller effective support ratio for a given certain infiltration distance. Figure 8 shows that for a certain tunnel diameter, cover depth has little influence on the effective support ratio.

## 3 SOIL LAYERING AND MICRO STABILITY

Soil layering may affect the pressures at the tunnel face and thus the stability of the tunnel face. Two common types of soil layering are shown in Figure 9. For an unconfined aquifer, a condition of homogeneous soil may be assumed. The piezometric head at the face can be approximated by (Bezuijen, 2001):

$$\phi = \phi_0 \left[ \sqrt{1+(2x/D)^2} - 2x/D \right] \tag{14}$$

where $\phi$ the piezometric head (m) at a distance $x$ (m) in front of the tunnel face, $\phi_0$ is the piezometric head at the tunnel face (m), and $D$ (m) the tunnel diameter, assuming a piezometric head of zero far from the tunnel in the pore water.

Derivation of Equation (14) to $x$ leads to:

$$\frac{\mathrm{d}\phi}{\mathrm{d}x} = \frac{2\phi_0}{D}\left( \frac{x}{\sqrt{x^2+(D/2)^2}} - 1 \right) \tag{15}$$

At the tunnel face $x = 0$, we have:

$$i = \frac{\mathrm{d}\phi}{\mathrm{d}x}\Big|_{x=0} = -\frac{2\phi_0}{D} \tag{16}$$

For a semi-confined aquifer, the piezometric head at the face can be calculated with (Bezuijen & Xu, 2018):

$$\phi(r) = \frac{Q}{2\pi kH} K_0\left(\frac{r}{\lambda}\right) \tag{17}$$

where $Q$ is the discharge at the face ($m^3/s$), $k$ the permeability of the soil (m/s), $H$ the height of aquifer (m), $r$ the distance from the centre of the tunnel face (m), $\lambda$ the leakage length (m). $K_0$ is the modified Bessel function of zero kind, see Appendix A. Equation (17) is valid when the height of the aquifer is more or less equal to the tunnel diameter. Otherwise, the calculation by Bezuijen & Xu (2018) has to be followed.

An approximate gradient at the tunnel face $x = 0$ was given by Bezuijen & Xu (2018):

$$i = \frac{\mathrm{d}\phi}{\mathrm{d}r}\Big|_{r=0} = \frac{2\phi_0}{D}\,\frac{1}{1-(0.5D/H)[1-K_0(0.5H/\lambda]} \tag{18}$$

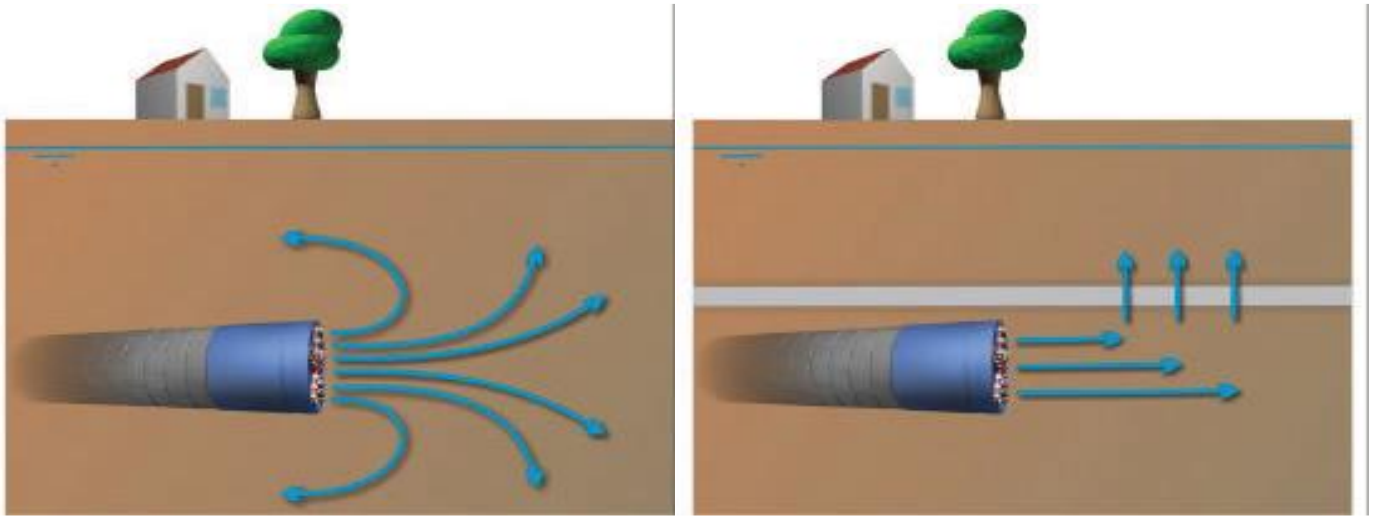


Figure 9. Sketch groundwater flow caused by shield tunnelling. (After COB, 1998, drawings by A. Bezuijen jr, used with permission)

To stabilise a vertical face of cohesionless sand, a constant drag force with a gradient of $i \geq 2$ has to be maintained (van Rhee & Bezuijen, 1992). Equations (16) and (18) show that a larger tunnel diameter leads a lower gradient. For a tunnel with diameter of 5 m or smaller in an unconfined aquifer, a support pressure of 50 kPa (piezometric head of 5 m) at the face will result in $i \geq 2$. This meets the minimum required gradient. However, in case of a tunnel with diameter of 10 m or larger, a gradient $i \leq 1$ will be achieved for a support pressure of 50 kPa in an unconfined aquifer. Therefore, support with pure water fails to stabilise the face. In a semi-confined aquifer, the condition will be more complicated. The gradient depends on the support pressure, the tunnel diameter, the height of aquifer and the leakage length. For a 10 m diameter tunnel in a 30 m high aquifer, a support pressure of 50 kPa (piezometric head of 5 m) a gradient $i < 2$ will be achieved at the face. This gradient is unable to achieve a stable body of cohesionless grains. For a 5 m diameter tunnel, the gradient will be larger than 2 and thus a stable tunnel face can be achieved

Apart from the micro-stability consequence, soil layering has some other influences in the stability: The excess pore water pressures and thus the infiltration in front of the TBM can be different for various soil layering. Bezuijen & Xu (2018) have shown that TBM excavation in a semi-confined aquifer leads to higher excess pore water pressures in the soil around the TBM during excavation. Furthermore, the high pore water pressures decrease the stability of the tunnel face and therefore an increased face pressure will be necessary compared to the unconfined situation. Bezuijen & Xu (2018) showed that for a semi-confined aquifer, the excess pore water pressures caused by drilling are present over a larger area than in an unconfined aquifer. This may increase the risk of a blowout (Aime et al. 2004). Furthermore, the infiltration velocity of the slurry in the soil in front of the TBM will be slower during both excavation and the standstill. Both the larger extent of the excess pore water pressures and the lower infiltration velocity of the slurry will decrease the stability of the tunnel face (Bezuijen & Xu, 2018).

## 4 CONCLUSIONS

Based on the analyses of macro- and micro- stability of the face of slurry shield-driven tunnel in an aquifer, the following conclusions may be allowed to be drawn.

The larger infiltration distance or the larger ratio of cover depth to the tunnel diameter ($C/D$) at a certain cover depth, the higher additional margin for the support pressure is required.

Soil layering influences the hydraulic gradient at the face and thus the face stability. In an unconfined aquifer, a larger tunnel leads to a lower hydraulic gradient at the face. In a semi-confined aquifer, a larger tunnel also leads to a lower gradient but the condition will be more complicated. It also depends on the height of aquifer and the leakage length etc. Generally, for a tunnel with the same diameter and support pressure, the gradient at the face in an unconfined aquifer will be higher than that in a semi-confined aquifer.

Furthermore, TBM excavating in a semi-confined aquifer leads to higher excess pore water pressures in the soil around the TBM and a reduced infiltration

of slurry into the soil in front of the TBM during both excavation and the standstill; The excess pore water pressures are present over a larger area, increasing the risk of a blow-out during excavation.

## ACKNOWLEDGEMENT

The research is funded supported by Science and Technology Development Fund, Macao Special Administrative Region of China (File numbers: FDCT/0035/2019/A1 and FDCT/193/2017/A3).

## REFERENCES

Aime, R., Aristaghes, P., Autuori, P., Minec, S. 2004. 15 m diameter tunneling under Netherlands polders. In: ITA Proceedings of Underground Space for Sustainable Urban Development, Singapore, Elsevier.

Ahmed, M. & Iskander, M. 2012. Evaluation of tunnel face stability by transparent soil models. *Tunnelling and Underground Space Technology*, 27 (1), 101-110.

Anagnostou, G. & Kovári, K. 1994. The face stability of slurry-shield-driven tunnels. *Tunnelling and Underground Space Technology*, 9 (2): 165-174.

Bezuijen, A., 1996. Inventarisatie Boorprojecten met "Loopzand". Technical Report 15, Boren Tunnels en Leidingen.

Bezuijen A., Pruiksma J.P., Meerten H.H. van, 2001. Pore pressures in front of tunnel, measurements, calculations and consequences for stability of tunnel face. Proc. Int. Symp. on Modern Tunneling Science and Techn. Kyoto.

Bezuijen, A., Steeneken, S. P., Ruigrok, J. A. T., 2016. Monitoring and analysing pressures around a TBM, In: The 13th International Conference Underground Construction, Prague.

Bezuijen, A. & Xu, T. 2018. Excess pore water pressures in front of a tunnel face when drilling in a semiconfined aquifer. *ITA-AITES World Tunnel Congress*, Dubai, 2-10.

Broere, W. 2001. *Tunnel Face Stability & New CPT Applications*. Ph.D. thesis, Delft University of Technology, Delft, The Netherlands.

Broere, W. 2015. On the face support of microtunnelling TBMs. *Tunnelling and Underground Space Technology* 46, 12-17.

Broere, W., van Tol, A. 2001. Time-dependant infiltration and groundwater flow in a face stability analysis. In: Adachi, T., Tateyama, K., Kimura, M. (Eds.), *Modern Tunneling Science and Technology*. Balkema, 629-634.

Chambon, P., Corté, J., Garnier, J., König, D. 1991. Face stability of shallow tunnels in granular soils. In: Ko, H., McLean, F. (Eds.), *Centrifuge '91*. Balkema, Rotterdam, 99-105.

Chen, R. P., Li, J., Kong, L. G., Tang, L. J. 2013. Experimental study on face instability of shield tunnel in sand *Tunnelling and Underground Space Technology* 33: 12-21.

COB (Centre for Underground Construction).(2000. *Second Heinenoord tunnel evaluation report*, COB report K100-06. Gouda, The Netherlands: COB.

Horn, N. 1961. Horizontaler Erddruck auf senkrechte Abschlussflächen von Tunnelröhren. In: *Landeskonferenz der Ungarischen Tiefbauindustrie*, 7-16.

Hölscher, P. 2008. *Procesverbetering Aanleg Ondergrondse Infrastructuur –Microtunnelling*. Technical Report TC161, Centrum Ondergronds Bouwen. G.

Jancsecz, S. & Steiner, W. 1994. Face support for a large mix-shield in heterogenous ground conditions. In: *Tunneling '94, Institution of Mining and Metallurgy*, London, 531-550.

Liu, X. Y., Wang, F. M., Fang, H. Y., Yuan, D. J. 2019. Dual-failure-mechanism model for face stability analysis of shield tunneling in sands. *Tunnelling and Underground Space Technology* 85: 196-208.

Perazzelli, P., Leone, T., Anagnostou, G. 2014. Tunnel face stability under seepage flow conditions. *Tunnelling and Underground Space Technology* 43: 459-469.

Qarmout, M., König, D., Gussmann, P., Thewes, M., Schanz, T. 2019. Tunnel face stability analysis using Kinematical Element Method. *Tunnelling and Underground Space Technology* 85, 354–367.

van Rhee, C. & Bezuijen, A. 1992. Influence of seepage on stability of sandy slope. *ASCE Journal of Geotechnical Engineering* 8: 1236-1240.

Xu, T. & Bezuijen, A. 2018. Analytical methods in predicting excess pore water pressure in front of slurry shield in saturated sandy ground. *Tunnelling and Underground Space Technology* 73: 203-211.

Xu, T. & Bezuijen, A. 2019. Bentonite slurry infiltration in sand: filter cake formation under various conditions. *Géotechnique*, 69 (12), 1095-1106.

Zizka, Z. & Thewes, M. 2016. *Recommendations for face support pressure calculations for shield tunnelling in soft ground*. Cologne, Germany: Deutscher Ausschuss fuer unterirdisches Bauene. V. German Tunnelling Committee (ITA-AITES).

Zhang, C., Han, K., Zhang, D. 2015. Face stability analysis of shallow circular tunnels in cohesive–frictional soils. *Tunnelling and Underground Space Technology*, 50, 345-357.

## APPENDIX A

$$K_0(x) = -\{\ln(x/2) + \gamma\} I_0(x) + \sum_{m=1}^{\infty} \frac{(x/2)^{2m}}{(m!)^2 (1 + \frac{1}{2} + \frac{1}{3} + \cdots + \frac{1}{m})} \quad (1)$$

$$I_0(x) = \sum_{m=0}^{\infty} \frac{(x/2)^{2m}}{m!\,\Gamma(m+1)} = \sum_{m=0}^{\infty} \frac{(x/2)^{2m}}{(m!)^2} \quad (2)$$

$$\Gamma(m) = (m-1)! \ (m = 1,\ 2,\ 3,\ \ldots) \quad (3)$$